Calculation of dike trajectories from volcanic centers

Catherine Mériaux[1] and John R. Lister

Institute of Theoretical Geophysics, Department of Applied Mathematics and Theoretical Physics, University of Cambridge, Cambridge, UK

Received 11 May 2000; revised 13 August 2001; accepted 18 August 2001; published 26 April 2002

[1] Patterns of dike swarms around volcanic centers or above mantle plumes are interpreted by a mechanical analysis of regional and dike-induced stresses, in which dike emplacement is controlled and guided by the stress state. Comparisons of dike patterns with patterns of principal-stress trajectories caused by a source and a regional stress system are commonly used to infer paleostresses. However, dike trajectories are determined by a complex interaction between dike-induced stresses and the source/regional stress system. We present numerical calculations based on a novel boundary-integral formulation, which examines the simultaneous effects of regional stresses, magma pressure, and dike injection on the local stress state around a continuously curving dike. Dike paths are calculated from the condition that dikes propagate by mode I failure. Our results suggest that the magnitude of the regional stresses would be 2–5 times higher than previous estimates based on principal-stress trajectory analysis. *INDEX TERMS:* 8010 Structural Geology: Fractures and faults; 8020 Structural Geology: Mechanics; 8164 Tectonophysics: Stresses—crust and lithosphere; 8434 Volcanology: Magma migration; *KEYWORDS:* Dike swarm, propagation, dike path, principal-stress trajectory, regional stress

1. Introduction

[2] For many years, simple explanations of the mechanics and paths of dike intrusions have been developed from two basic statements [*Anderson*, 1951, pp. 21–25]. First, dikes open as a result of tensile loading exerted at the tip. Second, they select the orientation of "least resistance" by opening along planes across which the confining pressure is least. These statements established a connection between dike geometries and the ambient stress field [e.g., *Stevens*, 1911; *Anderson*, 1936, 1938; *Odé*, 1957] and led to the idea that dike paths simply trace trajectories perpendicular to the minimum compressive principal stress of the ambient stress field, i.e., the stress field present before dike propagation.

[3] This concept of principal-stress trajectories has been applied to dike swarms, which form characteristic geometrical patterns [e.g., *Odé*, 1957; *Muller and Pollard*, 1977; *Baer and Reches*, 1991; *McKenzie et al.*, 1992; *Koenig and Pollard*, 1998]. These patterns are observed on both Earth and Venus and are considered to be the result of subhorizontal propagation in different directions from a shallow source region (see *Ernst et al.* [1995] for a review). Maps of such dike swarms often show a systematic change in propagation direction with distance from a radial to a subparallel geometry. If the equivalence of dike paths and principal-stress trajectories is assumed, then the simple stress field due to a pressurized hole in an otherwise unstressed elastic body produces only a radial pattern. Thus the swarm patterns exhibiting a transition from radial to subparallel propagation suggest that a regional stress field existed in the crust at the time the dikes were injected. For example, calculations considering the superposition of the stress field due to a pressurized source and a biaxial regional stress field showed that reasonable agreement in pattern could be obtained by judicious choice of the relative magnitudes of the stresses [*Baer and Reches*, 1991; *McKenzie et al.*, 1992; *Koenig and Pollard*, 1998]. The transition from radial to subparallel geometry is located where the regional stress field begins to dominate that due to the pressurized source. Since reasonable geometrical fits and estimates of the remote shear stress can be obtained from such comparisons, the method has been considered reliable.

[4] However, these analysis are open to serious theoretical question because they ignore the fact that dikes radically alter the surrounding stress field as they propagate. The actual state of stress during propagation results from a complex interaction between the dike and its environment, in which both externally and internally generated stresses matter: the dike generates its own stress field through the distribution of magma pressure, which is related to the viscous pressure drop along its length; moreover, the presence of the dike (as a new internal structure) induces large changes in the local effects of the externally generated stresses. *McKenzie et al.* [1992] note that it is surprising that principal-stress trajectories give good agreement with observed patterns despite the neglect of these problems. Here we show that the full calculation gives at least as good qualitative agreement in pattern but substantially different estimates of the stresses.

[5] In the context of the mechanical interaction between neighboring joints or en echelon fractures, it has long been realized that crack-generated stresses change crack propagation paths from those predicted from remote stresses. Various studies have considered how the presence of one or more neighboring cracks influences the stress field near another and hence the propagation path [e.g., *Pollard et al.*, 1982; *Sempere and Macdonald*, 1986; *Olson and Pollard*, 1989; *Cruikshank et al.*, 1991; *Olson*, 1993; *Thomas and Pollard*, 1993]. These analyses largely focus on crack curvature as a crack-crack interaction effect caused by the approach and overlap of echelon segments. Here we apply similar considerations to the curvature of a single dike in an ambient stress field and show that the curvature is strongly influenced by the dike's self-interaction. Though we illustrate our analysis by application to radial dike swarms, we wish to emphasize the underlying concepts since these will also determine dike paths in other settings.

[6] Calculation of the effects of a propagating crack in an ambient stress field requires solution of an elastic problem in which the crack geometry is generally not a simple straight line or circular arc but an arbitrary continuously curving path. Several straight cracks can be dealt with by reflection techniques [*Pollard et al.*, 1982] and small deflections from a straight path can be dealt

[1]Now at Research School of Earth Sciences, Australian National University, Canberra, ACT, Australia.

0148-0227/02/2001JB000436$09.00

using the analysis of *Cotterell and Rice* [1980] [*Cruikshank et al.*, 1991]. However, previous calculations of propagation along more general curving trajectories [e.g., *Olson and Pollard*, 1989; *Olson*, 1993; *Thomas and Pollard*, 1993] have largely been based on the boundary element method of *Crouch and Starfield* [1983]. This method employs a simple discretization in which the dike shape is approximated by elements consisting of straight-line segments and the wall displacement on each element is taken to be constant. Thus there are discontinuities in both the crack direction and the wall displacement at the joins between the elements, and propagation proceeds in a series of small kinks. We have reformulated the problem in terms of a boundary integral equation and developed a smoother and much more accurate representation in which the boundary elements are circular arcs and the boundary displacement is piecewise linear (see Appendix A). This allows the dike orientation and wall displacement to be continuous along the dike length and the propagation direction to change continously.

[7] We start by discussing the principles determining dike paths. We then illustrate our ideas by applying them to model patterns of dike swarms from a volcanic center.

2. Criteria for a Dike Path

[8] In theoretical mechanics, crack propagation is usually analyzed in terms of three basic modes, which are distinguished by the type of loading exerted at the crack tip: mode I, or opening mode, refers to purely tensile loading of the crack tip; mode II, or sliding mode, and mode III, or tearing mode, refer to pure shear loading of the crack tip, respectively, perpendicular to and parallel to the front. A superposition of more than one type of loading is termed mixed-mode propagation. In linear elastic fracture mechanics, these three modes are associated with stress intensity factors, K_{I}, K_{II}, and K_{III}, which are defined by the form of the near-tip stress and displacement fields

$$\sigma_{ij} \sim r^{-1/2} \sum_{m=1}^{\mathrm{III}} K_m f_{mij}(\theta) \tag{1}$$

$$u_i \sim r^{1/2} \sum_{m=1}^{\mathrm{III}} K_m g_{mi}(\theta), \tag{2}$$

where r is the radial distance from the crack tip and $f(\theta)$ and $g(\theta)$ are functions of angle θ [*Lawn*, 1993, p. 26].

[9] If a crack tip is subject to mixed-mode loading, then its incremental direction of propagation will make a nonzero angle, or kink, with the tangent direction at the previous tip position [*Erdogan and Sih*, 1963]. The kink angle is determined by the requirement that the loading of the incremented tip is mode I (equivalently, by the maximum circumferential stress criterion). Moreover, it follows that if the subsequent propagation path curves smoothly (without further kinks), then the tip loading must be such that fracture proceeds in pure mode I [*Cotterell and Rice*, 1980], and this determines the curvature. Thus smoothly curving dikes propagate along the path for which the only nonzero stress intensity factor is K_{I}. The stress intensity factors, and hence this "mode I path," are determined by the integrated effects of the loading of the dike walls by both internal and remote stresses. The loading can be resolved into normal and tangential components,

$$\sigma_n = P_m - \left[\sin^2\alpha\sigma_{xx} + \cos^2\alpha\sigma_{yy} - 2\sin\alpha\cos\alpha\sigma_{xy}\right] \tag{3a}$$

$$\sigma_t = -\left[\left(\sin^2\alpha - \cos^2\alpha\right)\sigma_{xy} - \cos\alpha\,\sin\alpha\left(\sigma_{yy} - \sigma_{xx}\right)\right], \tag{3b}$$

where α is the angle between the tangent to the crack and the x axis; σ_{xx}, σ_{yy}, and σ_{xy} are the components of the background remote stress field (with tension positive); P_m is the magmatic pressure, which decreases along the dike due to the viscous resistance to flow which determines the propagation rate [*Lister*, 1990; *Lister and Kerr*, 1991].

[10] To illustrate the difference between a principal-stress path and the mode I path, we begin with the very simple analytic example

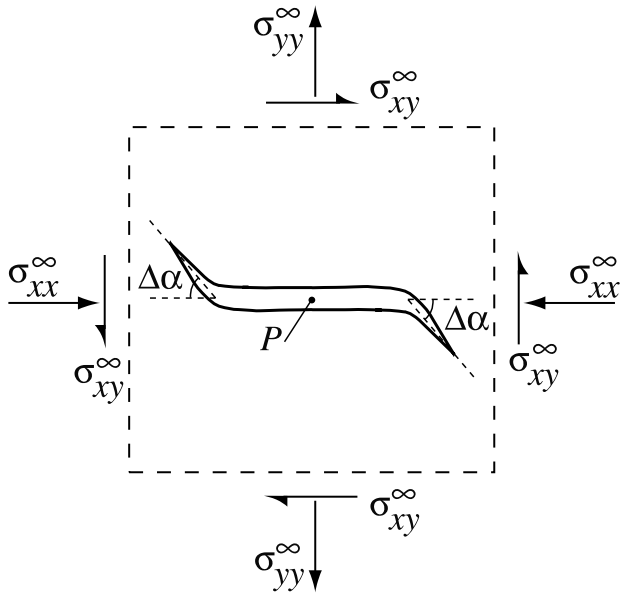

Figure 1. Initial extension and kink at angle $\Delta\alpha$ of a preexisting two-dimensional straight crack aligned with the x axis with constant internal pressure P in the presence of constant far-field stresses σ^{∞}_{xx}, σ^{∞}_{yy}, and σ^{∞}_{xy}.

of a straight crack starting to extend in an ambient stress field of uniform far-field stress. We suppose that the crack is initially aligned with the x axis with constant internal pressure P, that the far-field stresses are σ^{∞}_{xx}, σ^{∞}_{yy}, and σ^{∞}_{xy} and that $\sigma^{\infty}_{xy} \neq 0$ so that the crack will deviate from the x axis as it starts to propagate (Figure 1).

[11] To make a point, we define the principal-stress trajectories in terms of the ambient far-field stresses and think of the initial crack as the result of more recent propagation whose effects on the preexisting stress are ignored. The principal-stress trajectories are then straight lines at an angle $\Delta\alpha$ to the x axis, where

$$\tan(2\Delta\alpha) = \frac{2\sigma^{\infty}_{xy}}{\sigma^{\infty}_{xx} - \sigma^{\infty}_{yy}}. \tag{4}$$

Thus the principal-stress approach predicts that the dike kinks and then propagates in a straight line at this angle, which depends only on the far-field stresses and not on the orientation or internal pressure of the original crack.

[12] The mode I path can be calculated using results from equation (31) of *Cotterell and Rice* [1980], who considered a crack subjected to a combination of mode I and mode II loading at the initial tip; if the local stress field at the incremented tip position is required to be purely mode I (i.e., $K^{\mathrm{inc}}_{\mathrm{II}} = 0$) then the crack must kink by an angle $\Delta\alpha$, where

$$\frac{\sin(\Delta\alpha/2) + \sin(3\Delta\alpha/2)}{\cos(\Delta\alpha/2) + 3\cos(3\Delta\alpha/2)} = -\frac{K^0_{\mathrm{II}}}{K^0_{\mathrm{I}}} \tag{5}$$

and K^0_{I} and K^0_{II} are the stress intensity factors at the tip of the initial crack. Equation (5) depends explicitly on K^0_{I} and K^0_{II}, since it is the dominant $r^{-1/2}$ near-tip stress field (equation (2)) that determines the path. For the initially straight crack with constant far-field stresses, $K^0_{\mathrm{I}} = \sigma_n\sqrt{\pi l}$ and $K^0_{\mathrm{II}} = \sigma_t\sqrt{\pi l}$ [*Lawn*, 1993], where $\sigma_n = \sigma^{\infty}_{yy} - P$ and $\sigma_t = \sigma^{\infty}_{xy}$, and l is the crack half length. Thus equation (5) can be rewritten as

$$\frac{\sin(\Delta\alpha)}{3\cos(\Delta\alpha) - 1} = \frac{\sigma^{\infty}_{xy}}{P - \sigma^{\infty}_{yy}} \tag{6}$$

which coincides with the maximum-stress criterion of *Erdogan and Sih* [1963]. It should be noted that after the initial kink the crack propagates along a curved trajectory, since the extension of the crack modifies the near-tip field and hence the direction of propagation for the next increment. This curvature is in agreement with observations in mechanical samples [*Lawn*, 1993].

[13] Comparison of equations (4) and (6) shows that the principal-stress and mode I paths are significantly different for the straightforward reason that the principal-stress criterion is based entirely on the orientation of the stresses that would be at the position of the crack tip if there were no crack present. However, the introduction of the crack as an internal surface free of shear stress completely changes the stresses at the location of the tip from a constant background stress to the singular stress concentration of equation (2). An improved principal-stress prediction could be obtained if the stress field around the initial crack were considered part of the ambient stress field when calculating the trajectories for the subsequent propagation. However, the method would still be increasingly inaccurate as the crack propagates from its original position and changes the stress field from the initial stress field used to calculate the trajectories. In contrast, the mode I criterion defines the crack path in terms of the actual stresses at the propagating tip and is clearly much more physically reasonable.

3. Example: Propagation From a Volcanic Center

[14] In order to illustrate the geological significance of the difference between principal-stress predictions and mode I paths, we now focus on the pattern of dike swarms radiating from a volcanic center.

3.1. Regional Stress Field

[15] Models of the stress field around a volcanic center have previously been used to predict principal-stress trajectories and then to infer the regional stress field from the observed dike paths. The common parameterization of the stress field is based on the two-dimensional problem of a pressurized circular hole, representing the magmatic source, in an elastic body subject to a constant far-field biaxial stress, representing the regional stresses (Figure 2). For a hole of internal pressure P and a biaxial far-field stress composed of an isotropic mean stress M and a differential stress $2S$ (with tension again positive), the analytic solutions [*Kirsch*, 1898; *Jaeger and Cook*, 1979] for the stresses in Cartesian coordinates are

$$\sigma_{xx} = M - S - [P + M - 2S]\left(\frac{R}{r}\right)^2 \cos 2\theta - S\left[3\left(\frac{R}{r}\right)^4 - 2\left(\frac{R}{r}\right)^2\right]\cos 4\theta, \quad (7a)$$

$$\sigma_{yy} = M + S + [P + M + 2S]\left(\frac{R}{r}\right)^2 \cos 2\theta + S\left[3\left(\frac{R}{r}\right)^4 - 2\left(\frac{R}{r}\right)^2\right]\cos 4\theta, \quad (7b)$$

$$\sigma_{xy} = -[P + M]\left(\frac{R}{r}\right)^2 \sin 2\theta - S\left[3\left(\frac{R}{r}\right)^4 - 2\left(\frac{R}{r}\right)^2\right]\sin 4\theta, \quad (7c)$$

where $r = \sqrt{x^2 + y^2}$, $\cos\theta = x/r$, $\sin\theta = y/r$, and R is the radius of the hole. The far-field stresses are $\sigma^{\infty}_{xx} = M - S$, $\sigma^{\infty}_{yy} = M + S$, and $\sigma^{\infty}_{xy} = 0$; the terms involving P are just isotropic dilation from a source with overpressure $P + M$ (which take the simple form $\sigma_{rr} = -(P + M)(R/r)^2$, $\sigma_{\theta\theta} = (P + M)(R/r)^2$, $\sigma_{r\theta} = 0$ in cylindrical coordinates); the remaining terms involving S represent the perturbation to the far-field stress due to the presence of the hole and are required to satisfy the constant-pressure boundary conditions $\sigma_{rr} = -P$ and $\sigma_{r\theta} = 0$ on $r = R$. *Koenig and Pollard* [1998] calculate their principal-stress trajectories from equation (7).

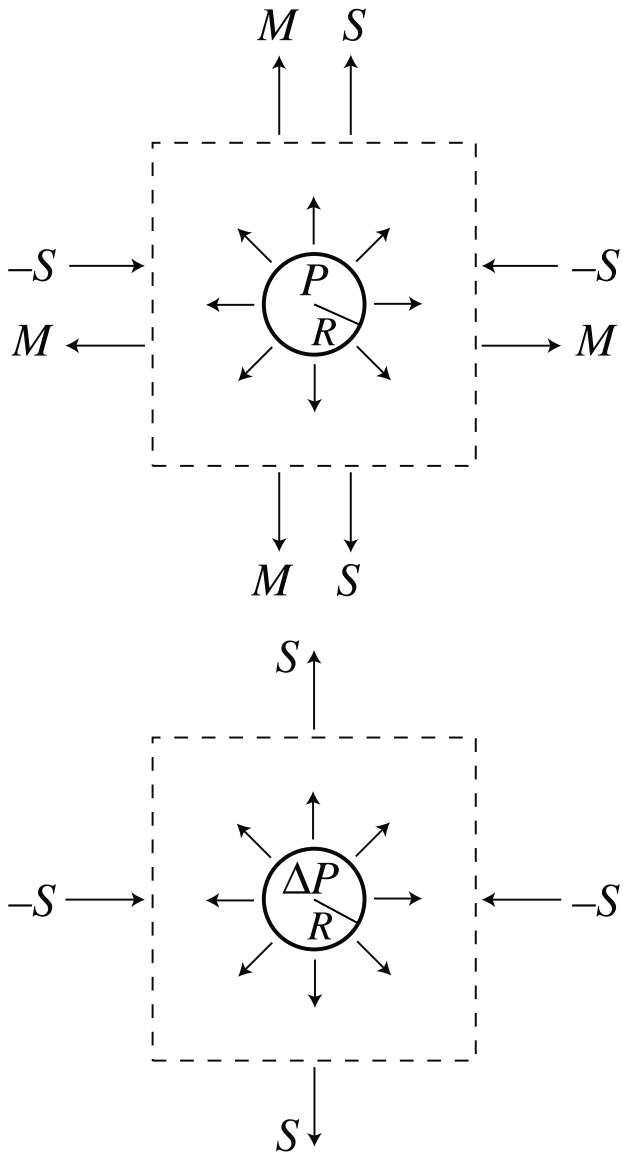

Figure 2. (top) Circular hole of radius R and internal pressure P in an elastic body subject to a biaxial stress at infinity split into an isotropic mean stress field M and a deviatoric stress field of magnitude S. (bottom) Circular hole of overpressure ΔP in an elastic body subject to a deviatoric remote stress of magnitude S.

[16] In simplified versions of equation (7) [*Odé*, 1957; *Muller and Pollard*, 1977; *Baer and Reches*, 1991; *McKenzie et al.*, 1992] the stresses are approximated by

$$\sigma_{xx} \approx -S - \Delta P\left(\frac{R}{r}\right)^2 \cos 2\theta, \quad (8a)$$

$$\sigma_{yy} \approx S + \Delta P\left(\frac{R}{r}\right)^2 \cos 2\theta, \quad (8b)$$

$$\sigma_{xy} \approx -\Delta P\left(\frac{R}{r}\right)^2 \sin 2\theta, \quad (8c)$$

as discussed below.

[17] In moving from equation (7) to equation (8), two simplifications are made. First, addition of a uniform isotropic stress does not affect the principal-stress trajectories, and so the uniform far-field mean stress M can be subtracted from σ_{xx} and σ_{yy}. It is

important then to remember both that the stresses σ_{ij} in equation (8) denote the deviations from the mean compression and not the true stresses of equation (7) and that the source pressure ΔP is the source overpressure $P + M$ and not the actual source pressure P. *Koenig and Pollard* [1998] criticize *McKenzie et al.* [1992] for setting the remote mean stress equal to zero by using (8) and thus ignoring the effect of mean stress on trajectories. In fact, there is no problem here provided the pressure P in *McKenzie et al.* [1992] is understood to be the overpressure relative to the mean stress and not the actual pressure (the paper does not explicitly define P). Thus equation (7) can be rewritten as

$$\frac{\Delta\sigma_{xx}}{S} = -1 - \left[\frac{\Delta P}{S} - 2\right]\left(\frac{R}{r}\right)^2 \cos 2\theta - \left[3\left(\frac{R}{r}\right)^4 - 2\left(\frac{R}{r}\right)^2\right]\cos 4\theta, \tag{9a}$$

$$\frac{\Delta\sigma_{yy}}{S} = 1 + \left[\frac{\Delta P}{S} + 2\right]\left(\frac{R}{r}\right)^2 \cos 2\theta + \left[3\left(\frac{R}{r}\right)^4 - 2\left(\frac{R}{r}\right)^2\right]\cos 4\theta, \tag{9b}$$

$$\frac{\Delta\sigma_{xy}}{S} = -\frac{\Delta P}{S}\left(\frac{R}{r}\right)^2 \sin 2\theta - \left[3\left(\frac{R}{r}\right)^4 - 2\left(\frac{R}{r}\right)^2\right]\sin 4\theta, \tag{9c}$$

showing that the problem only depends on R and the relative magnitudes of the remote stress S and the overpressure ΔP; here S is taken to be positive by choice of the x and y axes, and ΔP is assumed to be positive since we are interested in radial near-field trajectories. (Negative ΔP produces circumferential propagation and ring dikes.)

[18] The second simplification rests on an implicit assumption that $S \ll \Delta P$. If this is the case, then the stresses due to the hole overpressure ΔP are dominant in the near field ($r \approx R$) and the near-field perturbation to the ambient differential stress caused by the presence of the hole (i.e., terms in equation (7) proportional to $S(R/r)^m \cos(n\theta)$ with $m, n = 2$ or 4) can be neglected to reduce equation (9) to equation (8). The dominant stresses due to the hole overpressure produce radial propagation in the near field. These stresses decrease with radial distance and are equal to the ambient biaxial stress at radius r^*, where $r^* = R(\Delta P/S)^{1/2}$. It is thus to be expected that the dike swarm will curve toward a subparallel geometry at this sort of radius. The assumption that $S \ll \Delta P$ could be justified either from observations that the dike swarm curves on a longer length scale than the source dimensions (for example, on Venus [*Grosfils and Head*, 1994]) or from modeling the swarm pattern and checking, a posteriori, that the best fit gives $S \ll \Delta P$. It seems to be a reasonable approximation in previous studies of volcanic centers [*Odé*, 1957; *Muller and Pollard*, 1977; *Baer and Reches*, 1991; *McKenzie et al.*, 1992] but would not be appropriate in tectonically active regions, like Iceland, where there are relatively large differential stresses and dike swarms are closely subparallel.

[19] For simplicity, we will also restrict our attention to cases in which the stress field can be approximated by equation (8) and note, for example, that the principal-stress trajectories are not much affected by the approximation even for values of $S/\Delta P$ as large as 0.5 (Figure 3). The field examples described in section 5 have $S/\Delta P \leq 0.25$.

3.2. Nondimensionalization

[20] The simplified stresses in equation (8) can conveniently be made dimensionless by defining

$$\tilde{\sigma} = \sigma/S \tag{10}$$

$$\tilde{r} = r/r^*, \tag{11}$$

where the length scale $r^* = R(\Delta P/S)^{1/2}$ is the radius at which the hole and biaxial stress fields have equal magnitude. The dimensionless stress field is then given by

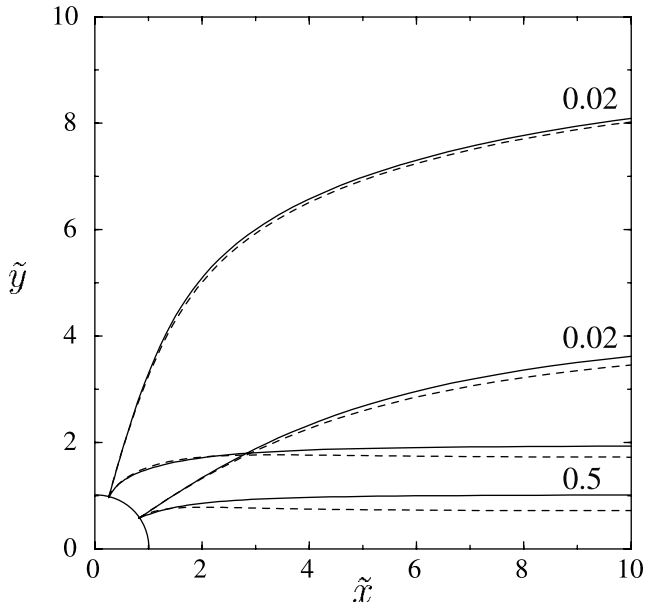

Figure 3. Some principal-stress trajectories calculated for the exact stress field (equation (7)) (dashed lines) and approximate stress field (equation (8)) (solid lines). Four trajectories are shown for each case corresponding to initial angles 35° and 75° and $S/\Delta P = 0.02$ and 0.5.

$$\tilde{\sigma}_{xx} = -1 - \frac{1}{\tilde{r}^2}\cos 2\theta, \tag{12a}$$

$$\tilde{\sigma}_{yy} = 1 + \frac{1}{\tilde{r}^2}\cos 2\theta, \tag{12b}$$

$$\tilde{\sigma}_{xy} = -\frac{2}{\tilde{r}^2}\sin 2\theta \tag{12c}$$

in $\tilde{r} > \tilde{R}$, where $\tilde{r} = R/r^* = (S/\Delta P)^{1/2}$ is the dimensionless hole diameter. Alternatively, $\tilde{R}^2$ can be thought of as the ratio of the regional differential stress to the source overpressure. This is the only parameter in the dimensionless problem, and we are interested in $\tilde{R} \ll 1$ (i.e., $R \ll r^*$).

3.3. Chamber Conditions

[21] The stress field in equation (12) is that appropriate for propagation from a pressurized source, or magma chamber, of dimensionless radius $\tilde{R}$. Though it would be possible to extend our calculations to include the chamber wall as an internal boundary with constant-pressure boundary conditions, it is simpler, and consistent with the approximations already made for $\tilde{R} \ll 1$ (i.e., $S \ll \Delta P$), to model the chamber by making the following approximations for $\tilde{r} < \tilde{R}$. We assume an initial state in which there is a straight dike of length $\tilde{R}$ at an angle α_0 to the x axis and extending from the origin to $\tilde{r} = \tilde{R}$ (Figure 4). We assume further that in $\tilde{r} < \tilde{R}$ the dike has a constant internal magmatic overpressure $\Delta\tilde{P}_m = 1/\tilde{R}^2$ and there is a constant stress field

$$\tilde{\sigma}_{xx} = -1 - \frac{1}{\tilde{R}^2}\cos 2\theta, \tag{13a}$$

$$\tilde{\sigma}_{yy} = 1 + \frac{1}{\tilde{R}^2}\cos 2\theta, \tag{13b}$$

$$\tilde{\sigma}_{xy} = -\frac{2}{\tilde{R}^2}\sin 2\theta. \tag{13c}$$

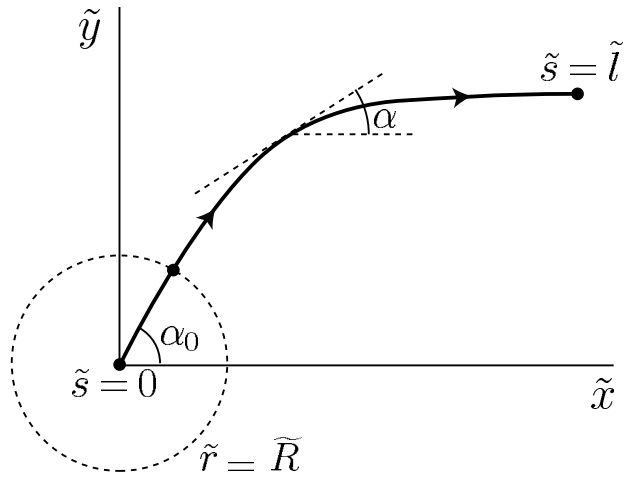

Figure 4. Curved dike path of length $\tilde{s} = l$. The propagation direction is defined by the tangent angle α with the x axis. The dike originates from a preexisting straight dike of length $\tilde{R}$ at an angle α_0 to the x axis.

We are concerned with dike curvature on length scales much greater than $\tilde{R}$ and the details of these approximations make little difference.

3.4. Magmatic Pressure Distribution

[22] When a dike propagates away from a source the magmatic overpressure decreases along the dike due to the dominant viscous resistance to flow [*Lister and Kerr*, 1991]. The detailed shape of the pressure profile in $\tilde{r} > \tilde{R}$ thus depends on the dike width and requires simultaneous solution of the equations of viscous flow and elastic deformation [e.g., *Spence and Turcotte*, 1985; *Lister*, 1990; *Rubin*, 1993a, 1993b]. For simplicity, we consider the end-member cases of constant magma overpressure ($\Delta\tilde{P}_m = 1/\tilde{R}^2$ in $\tilde{r} > \tilde{R}$) and a crack with no overpressure outside the chamber ($\Delta\tilde{P}_m = 0$ in $\tilde{r} > \tilde{R}$) and also the simple parameterization

$$\Delta\tilde{P}_m(\tilde{s}) = \frac{1}{\tilde{R}^2}\left[\frac{\tilde{l}-\tilde{s}}{\tilde{l}-\tilde{R}}\right]^{1/4} \quad \text{in } \tilde{r} > \tilde{R}, \tag{14}$$

where $\tilde{l}$ is the dimensionless length of the crack and $\tilde{s}$ is the dimensionless arc length along it; this parameterization approximates the shape of the pressure profile found in previous studies.

[23] We note that the initial dike configuration is subjected to a combination of mode I and mode II loading and thus kinks as it starts to propagate. Thereafter, the dike can curve smoothly along a mode I path.

3.5. Calculation of Mode I Propagation Paths

[24] We have argued that dikes follow a curving path which is determined by the condition that the tip loading is pure mode I, i.e., that $K_{II} = 0$ at every stage of propagation. In order to evaluate this path numerically, we use a stepwise method in which the dike path is considered to be a sequence of curved segments, which join smoothly to give a continuous variation of the propagation direction. At each propagation step the dike is extended from the previous tip by one segment. We calculate the value of K_{II} for trial additional segments and then choose the curvature of the additional segment so that $K_{II} = 0$ at the new dike tip. This tip condition can be expressed in terms of the tangential displacement of the dike walls using equation (2), and the wall displacements can in turn be found from the stress conditions of equation (3) on the dike walls using a boundary-integral formulation, as described in Appendix A. The value of K_I is always positive.

[25] Our calculations are for propagation of a single dike, though we present multiple trajectories in each plot to show the paths of dikes initiated at different angles. If many dikes are actually injected in a swarm, then it might be expected that the stresses induced by the early intrusions would affect the trajectories for later events. This could, in principle, be modeled if the temporal

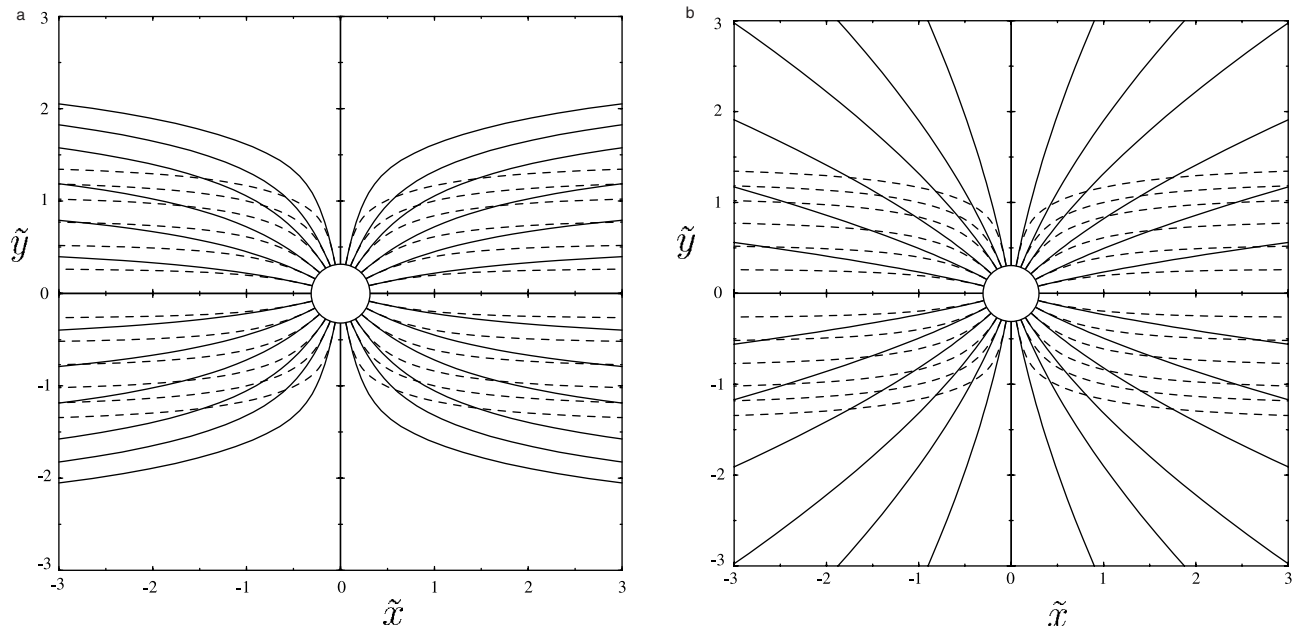

Figure 5. Dimensionless mode I dike paths (solid lines) and principal-stress trajectories (dashed lines) for $\tilde{R}^2 = S/\Delta P = 0.1$. Mode I paths for a crack with (a) no internal overpressure and (b) constant internal magma pressure $\Delta\tilde{P}_m = 1/\tilde{R}^2$.

order of the sequence of intrusions were known, together with the initial angle, volume, and propagation distance of each dike. However, the good agreement in pattern between the observed swarms and the multiple trajectories for a single dike suggests that the crustal stresses around each dike might relax sufficiently after intrusion not to affect subsequent intrusions.

4. Results

[26] In section 2 we showed analytically that the direction of extension of a straight crack in a regional stress field is predicted quite differently by principal-stress and mode I criteria. The same principle also applies to dike propagation from a volcanic center, but the mode I path can no longer be found analytically and numerical calculation is required. We explore the difference from principal-stress trajectories and the effects of the pressure distribution in the dike and of the parameter $\tilde{R}$.

[27] Figure 5 shows clearly that mode I dike paths, which are based on the actual near-tip stress fields, are significantly different from the principal-stress trajectories for the same regional stress field (equation (12)) with a given value of $\tilde{R}$. Even for a dike in which there is no magma overpressure on the dike walls in $\tilde{r} > \tilde{R}$ and the tip loading is due entirely to the applied regional stress and the chamber pressure, the mode I path propagates further in a radial direction before curving to be subparallel to the remote extension (Figure 5a). The effect is very much more marked for a dike loaded with uniform magma overpressure $\Delta\tilde{P}_m$ (Figure 5b), for which the curvature toward subparallel orientation occurs on a much longer scale than in the corresponding principal-stress trajectory.

[28] The dependence of the mode I dike paths on the distribution of magma overpressure is shown in Figure 6. Dikes with either uniform internal overpressure or with the simple parameterization in equation (14) of a viscous pressure drop propagate radially for much greater distances than the corresponding unpressurized cracks. The reason is simply that transmission of a magmatic overpressure from the source toward the dike tip provides a large tensile loading ahead of the tip; only a small curvature is then required to convert some of this tensile loading to sufficient shear loading to counterbalance the regional shear loading and maintain mode I propagation. For the same reason, uniformly loaded dikes tend to propagate with less curvature than those with a viscous pressure drop. The difference, however, is relatively small, suggesting that the parameterization in equation (14) is probably sufficient to get reasonable results without having to model the full details of the viscous flow in a curved dike of variable width.

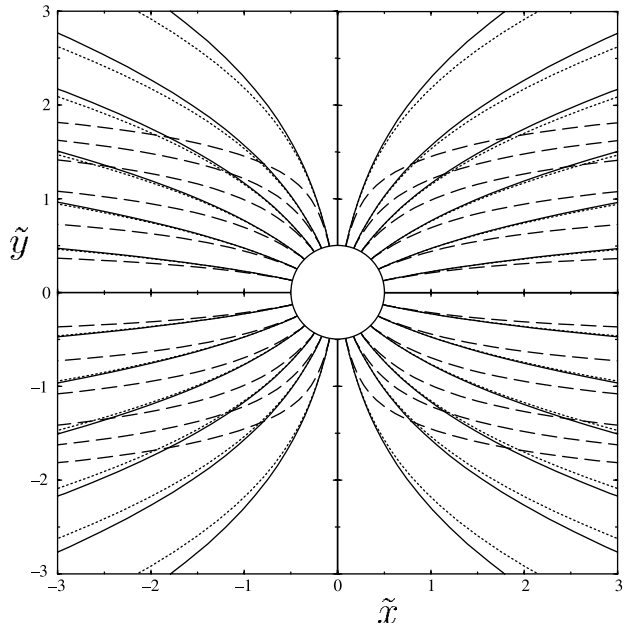

Figure 6. Dimensionless mode I dike paths for $\tilde{R}^2 = 0.25$ with three magmatic pressure distributions (see section 3.4): no magmatic overpressure outside the chamber (dashed lines), constant magmatic pressure (solid lines), and the simple parameterization in equation (14) of the viscous pressure drop (dotted lines).

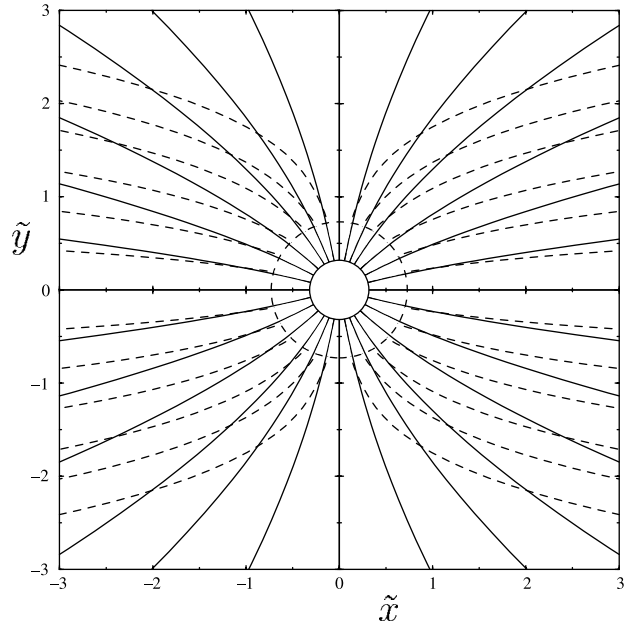

Figure 7. Dimensionless mode I dike paths for $\tilde{R}^2 = 0.1$ (solid lines) and $\tilde{R}^2 = 0.5$ (dashed lines), both with the simple parameterization (equation (14)) of the viscous pressure drop.

[29] While mode I paths curve much less than principal-stress trajectories for a given stress field, it should not be thought that large curvatures are not possible with mode I paths. Figure 7 shows the effects of varying $\tilde{R}$ for the most realistic pressure distribution in equation (14). An increase in $\tilde{R}$ produces mode I paths that curve more rapidly toward the principal direction of minimum compression since this corresponds to an increase in the remote differential stress relative to the overpressure in the source and propagating dike. Calculations with even larger values of $\tilde{R} = (S/\Delta P)^{1/2}$ should use a dimensionless version of the full stress field equation (7) rather than equation (12).

5. Application

[30] Studies of principal-stress trajectories were motivated by the idea that the remote differential stress could be estimated from fits between the principal-stress trajectories and the observed dike patterns. In practice, estimates of S are derived using the dimensionless parameter $\tilde{R}$ from

$$S = \tilde{R}^2\,\Delta P, \tag{15}$$

where $\tilde{R}$ is determined by the best fit between calculated trajectories and observed dike patterns and ΔP is estimated by other means. Larger curvatures correspond to larger values of $\tilde{R}$ and hence larger values of S for given ΔP. Since mode I paths curve less than principal-stress trajectories for a given $\tilde{R}$, the best fit mode I path will have a larger value of $\tilde{R}$ and hence give a larger value of S.

[31] For example, *Muller and Pollard* [1977] used the principal-stress trajectory approach on the West Peak intrusion, Colorado, to

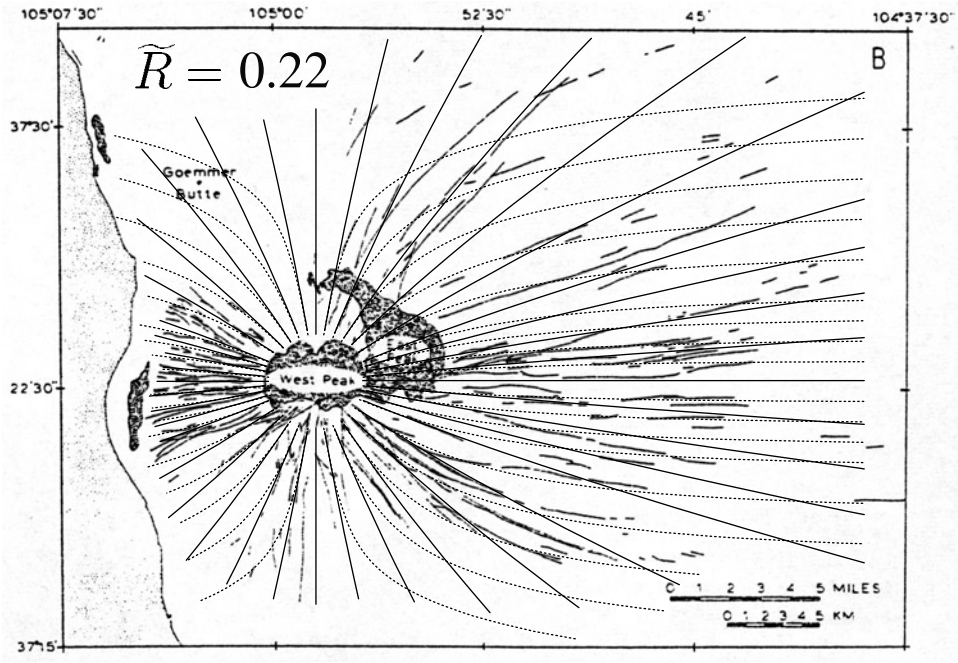

Figure 8. Observed pattern of dike segments at the Spanish Peaks region, Colorado, giving a reasonable fit with principal-stress trajectories (dashed lines) for $\tilde{R}$ = 0.22 [*Muller and Pollard*, 1977]. Mode I dike paths (solid lines) with this value of $\tilde{R}$ and the viscous pressure drop are quite different.

argue that the regional stress difference was <0.05 times the driving pressure (i.e., $\tilde{R}$ = 0.22). This value of $\tilde{R}$ gives a poor match between the mode I dike paths and observed dike trajectories (Figure 8). However, a very good match is obtained with the mode I paths for $\tilde{R}$ = 0.5 (Figure 9). This result implies that the remote stress S has an upper bound of 25 MPa rather than the previous estimate of 5 MPa.

[32] A second example is furnished by *Koenig and Pollard* [1998] study of a dike swarm on Venus. While they achieved a reasonably good fit between principal-stress trajectories and the

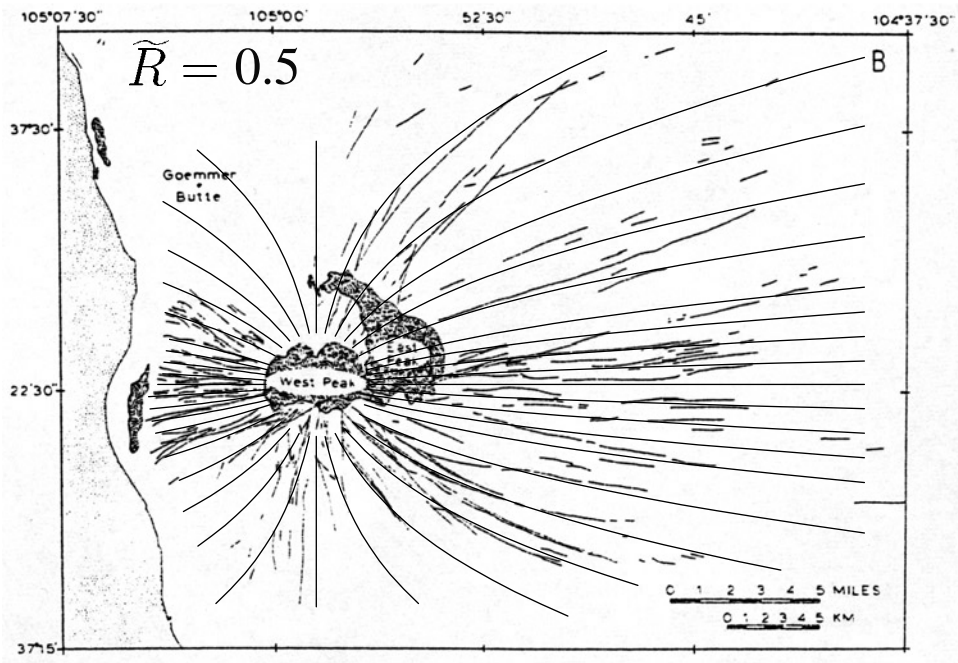

Figure 9. Mode I dike paths with the viscous pressure drop and $\tilde{R}$ = 0.5, giving very good agreement with the observed dike pattern at the Spanish Peaks region, Colorado.

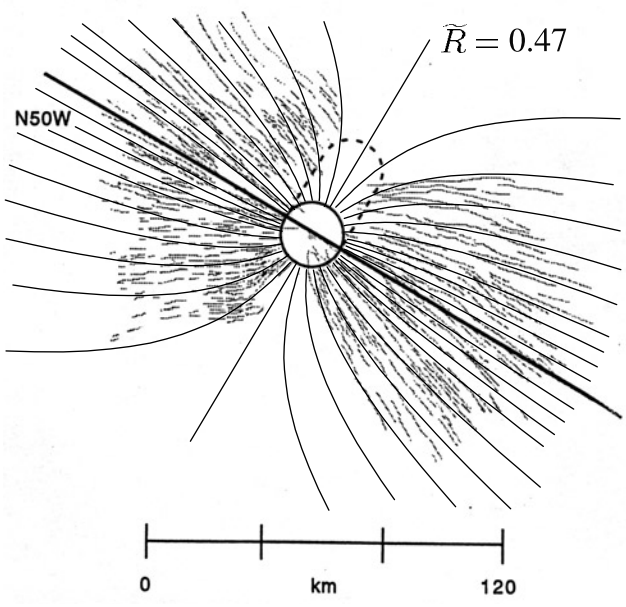

Figure 10. Mode I dike paths with the viscous pressure drop, giving good agreement for $\tilde{R}$ = 0.47 with the observed dike pattern in the Venusian swarm studied by *Koenig and Pollard* [1998].

observed dike pattern for $\tilde{R}$ = 0.33, our mode I calculations give at least as good a fit with $\tilde{R}$ = 0.47 (Figure 10). Therefore the estimate of S for a given magmatic overpressure from mode I dike paths is about double the estimate from principal-stress trajectories.

[33] These two examples show that both principal-stress trajectories and mode I paths can provide a good qualitative fit with the dike pattern. However, the inferred values of $S/\Delta P$ are quite different. Since the mode I path is based on the actual near-tip stress field, we consider it to be more reliable. More generally, we affirm that the use of dike paths as paleostress indicators is a powerful tool, but we emphasize the need to abandon the principal-stress approach.

6. Conclusion

[34] We have developed a description for dike propagation which is based on a well-defined and physically based criterion for the determination of the dike path, namely, that of mode I fracture. This criterion is well established for models of interacting fractures, but it is not commonly used for dike paths in a spatially varying ambient stress field. A simple numerical scheme allows calculation of dike paths with any prescribed loading. In particular, our results show that the magnitudes of regional differential stresses around volcanic centers are 2–5 times greater than previous estimates based on principal-stress trajectories. The general principle is that prediction of a dike trajectory requires calculation of the stress field near the dike tip as it propagates and cannot be directly inferred from the principal-stress directions prior to propagation.

[35] This work could be extended in a number of directions. For small driving pressures relative to the differential stress the full stress field (equation (7)) should be used, and walls of the magma chamber should be included as a free boundary in the boundary-integral formulation. Considerations of the circumferential stress in the chamber walls could then address the limited angular range occupied by many dike swarms. Second, it would be interesting to consider models of multiple intrusion in which the stress field from early emplaced dikes influence the paths of those emplaced later in the swarm. Finally, it should be noted that the lateral intrusion of dikes is not really a simple two-dimensional problem but may require some consideration of the vertical structure [e.g., *Rubin and Pollard*, 1987; *Lister*, 1990; *Bolchover and Lister*, 1999]. A fully three-dimensional calculation incorporating the vertical structure of the crust and allowing for propagation of all points around the perimeter of the dike plane would be a substantial undertaking. However, the principle that propagation is determined by the stress field at the dike tip during propagation will still hold.

Appendix A: Numerical Method

A1. Boundary-Integral Formulation

[36] The two-dimensional (2-D) problem of a curved crack with prescribed wall stresses is a standard boundary value problem in linear elasticity [e.g., *Crouch and Starfield*, 1983; *Muskhelishvili*, 1963; *Tanaka et al.*, 1994; *Mogilevskaya*, 1997], which can be expressed as an integral equation in a variety of forms [*Chen*, 1993]. In one of these, the "dislocation density method," the problem is written in the form

$$\int_C \mathbf{K}(\mathbf{x},\mathbf{s}) \begin{pmatrix} \partial h_x(\mathbf{s})/\partial s \\ \partial h_y(\mathbf{s})/\partial s \end{pmatrix} ds = \begin{pmatrix} \sigma_n(\mathbf{x}) \\ \sigma_t(\mathbf{x}) \end{pmatrix}, \tag{A1}$$

which expresses the known stresses at vector position $\mathbf{x}$ on the crack as an integral over the crack contour C of the derivatives of the unknown components $h_x(\mathbf{s})$ and $h_y(\mathbf{s})$ of the wall displacement. The kernel $\mathbf{K}(\mathbf{x}, \mathbf{s})$ is a 2×2 matrix, the integration variable s is the arc length along the crack, and $\mathbf{s}$ is the corresponding vector position. The additional constraint

$$\int_C \begin{pmatrix} \partial h_x(\mathbf{s})/\partial s \\ \partial h_y(\mathbf{s})/\partial s \end{pmatrix} ds = \begin{pmatrix} 0 \\ 0 \end{pmatrix}, \tag{A2}$$

represents the condition that the crack is closed at both ends. The linear system of equations (A1) and (A2) is sufficient to determine unique solutions for h_x and h_y from the distributions of σ_n and σ_t along the crack.

[37] The wall displacement h has square-root singularities at the crack tips corresponding to the singularity in the displacement field (equation (2)) as $r \to 0$. We treat these singularities explicitly by writing

$$\frac{\partial h}{\partial s} = \frac{D(s)}{\sqrt{s(l-s)}}, \tag{A3}$$

where l is the length of the crack, and we have dropped the subscripts x and y for convenience. The new function $D(s)$ has no singularities and is much easier to treat numerically.

A.2. Discretization

[38] In order to solve equations (A1) and (A2) for $D(s)$ numerically, both the dike geometry and the function $D(s)$ are discretized along the dike contour C. The dike geometry is represented by elements consisting of circular arcs which are chosen to join smoothly at node points. (Two of the three parameters needed to define each additional circular arc are determined by matching the end-point location and tangent direction of the previous arc, leaving the third parameter, the curvature of the arc, to be determined by the mode I criterion.) The function $D(s)$ is represented by $D(s) = \sum_j D_j f_j(s)$, where the D_j are the values of $D(s)$ at node point j and the $f_j(s)$ are piecewise linear basis functions. We evaluate equation (A1) at the midpoints $\mathbf{x}_k$ of the elements. These

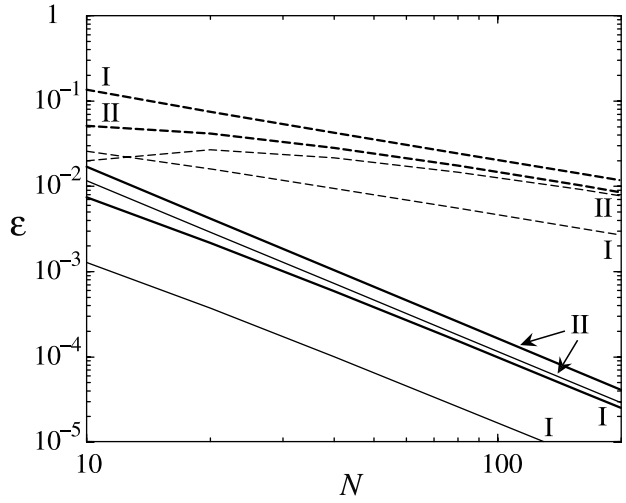

Figure A1. Relative error $\epsilon = |K_{num} - K_{exact}|/K_{exact}$ in the numerically determined stress intensities K_I and K_{II} at the tips of a circular arc crack of angle 2α subject to uniform far-field tension for $\alpha = 45°$ (thin lines) and $\alpha = 90°$ (thick lines) as a function of the number of boundary elements N. The present scheme (solid lines) is much more accurate than that of *Crouch and Starfield* [1983] as described by *Thomas and Pollard* [1993] (dashed lines).

representations reduce the problem to a linear system of algebraic equations

$$\sum_j D_j \int \frac{f_j(s)}{\sqrt{s(l-s)}} \mathbf{K}(\mathbf{x}_k, \mathbf{s}) ds = \sigma_k \qquad \text{(A4)}$$

$$\sum_j D_j \int \frac{f_j(s)}{\sqrt{s(l-s)}} ds = 0 \qquad \text{(A5)}$$

for the unknown displacements D_j in terms of the known midpoint stresses $\sigma_k = \sigma(\mathbf{x}_k)$.

A.3. Numerical Procedure

[39] The numerical code has three main parts. The first part consists of calculations of the integrals of the basis functions in equations (A4) and (A5) for a given geometry C. This requires careful treatment of the singularity at the pole of the Cauchy-type kernel $\mathbf{K}$, using singularity removal techniques [*Tanaka et al.*, 1994; *Pozrikidis*, 1992]. The second part constructs and inverts the matrix representing the linear system of equations to obtain the solution for D with this geometry and loading. In the third part, these two subroutines are nested within a root-finding algorithm which finds the curvature of the next circular arc to be added as the crack propagates from the condition that the tangential component $D_t = 0$ at the new tip; this corresponds to ensuring that $K_{II} = 0$.

A.4. Verification and Accuracy

[40] The numerical scheme was tested by comparison with the exact solution for a crack forming a circular arc subtending an angle 2α under uniform far-field tension [*Muskhelishvili*, 1963, p. 524]. The displacements and stress intensities obtained numerically agreed with the exact solution to within ~1.7% for $N = 10$ elements and within ~0.1% for $N = 40$ elements. In fact, the numerical error in the present scheme is proportional to N^{-2}. Direct implementation of the *Crouch and Starfield* [1983] scheme gives errors in displacement h proportional to $N^{-1/2}$ and overestimates the stress intensities by ~25% even if $N \to \infty$. The correction factor 0.806 used by *Thomas and Pollard* [1993] (0.798 is actually better) removes this leading-order error but still leaves numerical errors that are much greater than the present scheme (Figure A1). Thus fewer elements are needed in the present scheme for the same accuracy, or much greater accuracy can be achieved for the same N.

[41] **Acknowledgments.** We are very grateful to Richard Ernst, Jon Olson, and Allan Rubin for thorough and constructive reviews, which helped us improve the manuscript in many ways. This research has been supported by an EU Marie Curie Fellowship.

References

Anderson, E. M., The dynamics of the formation of cone-sheets ring-dykes and cauldron subsidences, *Proc. R. Soc. Edinburgh*, *56*, 128–157, 1936.
Anderson, E. M., The dynamics of sheet intrusion, *Proc. R. Soc. Edinburgh*, *58*, 242–251, 1938.
Anderson, E. M., *The Dynamics of Faulting and Dyke Formation With Applications to Britain*, Oliver and Boyd, White Plains, N. Y., 1951.
Baer, G., and Z. Reches, Mechanics of emplacement and tectonic implications of the Ramon dike systems, Israel, *J. Geophys. Res.*, *96*, 11,895–11,910, 1991.
Bolchover, P., and J. R. Lister, The effects of solidification on fluid-driven fracture, with application to bladed dykes, *Proc. R. Soc. London, Ser. A*, *455*, 2389–2409, 1999.
Chen, Y. Z., Numerical solution of a curved crack problem by using hypersingular integral equation approach, *Eng. Fract. Mech.*, *46*, 275–283, 1993.
Cotterell, B., and J. R. Rice, Slightly curved or kinked cracks, *Int. J. Fract.*, *16*, 155–169, 1980.
Crouch, S. L., and A. M. Starfield, *Boundary Element Methods in Solid Mechanics*, Allen and Unwin, Concord, Mass., 1983.
Cruikshank, K. M., G. Zhao, and A. M. Johnson, Analysis of minor fractures associated with joints and faulted joints, *J. Struct. Geol.*, *13*, 865–886, 1991.
Erdogan, F., and G. C. Sih, On the crack extension in plates under plane loading and transverse shear, *Trans. Am. Soc. Mech. Eng.*, *85*, 519–527, 1963.
Ernst, R. E., J. W. Head, E. Parfitt, E. Grosfils, and L. Wilson, Giant radiating dyke swarms on Earth and Venus, *Earth Sci. Rev.*, *39*, 1–58, 1995.
Grosfils, E., and J. W. Head, The global distribution of giant radiating dike swarms on Venus: Implications for the global stress state, *Geophys. Res. Lett.*, *21*, 701–704, 1994.
Jaeger, J. C., and N. G. W. Cook, *Fundamentals of Rock Mechanics*, 593 pp., Chapman and Hall, New York, 1979.
Kirsch, G. L., Die theorie der elastizitat und die bedurfnisse der festigkeitslehre, *Veit. Ver. Deut. Ing.*, *42*, 797–807, 1898.
Koenig, E., and D. D. Pollard, Mapping and modeling of radial fracture patterns, *J. Geophys. Res.*, *103*, 15,183–15,202, 1998.
Lawn, B. R., *Fracture of Brittle Solids* 2nd ed., Cambridge Univ. Press, New York, 1993.
Lister, J. R., Buoyancy-driven fluid fracture: Similarity solutions for the horizontal and vertical propagation of fluid-filled cracks, *J. Fluid. Mech.*, *217*, 213–239, 1990.
Lister, J. R., and R. C. Kerr, Fluid-mechanical models of cracks propagation and their applications to magma-transport in dikes, *J. Geophys. Res.*, *96*, 10,049–10,077, 1991.
McKenzie, D., J. M. McKenzie, and R. S. Saunders, Dike Emplacement on Venus and on Earth, *J. Geophys. Res.*, *97*, 15,977–15,990, 1992.
Mogilevskaya, S. G., Numerical modeling of 2-D smooth crack growth, *Int. J. Fract.*, *87*, 389–405, 1997.
Muller, O. H., and D. D. Pollard, Stress state near Spanish Peaks, *Pure Appl. Geophys.*, *115*, 69–86, 1977.
Muskhelishvili, N. I., *Some Basic Problems in the Mathematical Theory of Elasticity*, Wolters-Noordhoff, Groningen, Netherlands, 1963.
Odé, H., Mechanical analysis of the dike pattern of the Spanish Peaks area, Colorado, *Geol. Soc. Am. Bull.*, *68*, 567–576, 1957.
Olson, J. E., Joint pattern development: Effects of subcritical crack growth and mechanical crack interaction, *J. Geophys. Res.*, *98*, 12,251–12,265, 1993.
Olson, J., and D. D. Pollard, Inferring paleostresses from natural fracture patterns: A new method, *Geology*, *17*, 345–348, 1989.
Pollard, D. D., P. Segall, and P. T. Delaney, Formation and interpretation of dilatant echelon cracks, *Geol. Soc. Am. Bull.*, *93*, 1291–1303, 1982.
Pozrikidis, C., *Boundary Integral and Singularity Methods for Linearized Viscous Flow*, Cambridge Univ. Press, New York, 1992.
Rubin, A. M., Dikes vs. diapirs in viscoelastic rock, *Earth Planet. Sci. Lett.*, *119*, 641–659, 1993a.

Rubin, A. M., Tensile fracture of rock at high confining pressure: Implications for dike propagation, *J. Geophys. Res.*, *98*, 15,919–15,939, 1993b.

Rubin, A. M., and D. D. Pollard, Origins of blade-like dikes in volcanic rift zones, *U.S. Geol. Surv. Prof. Pap.*, *1350*, 1449–1470, 1987.

Sempere, J.-C., and K. C. Macdonald, Overlapping spreading centers: Implications from crack growth simulation by the displacement discontinuity method, *Tectonics*, *5*, 151–163, 1986.

Spence, D. A., and D. L. Turcotte, Magma-driven propagation of cracks, *J. Geophys. Res.*, *90*, 575–580, 1985.

Stevens, B., The laws of intrusions, *Bull. Am. Inst. Min. Eng.*, *41*, 1–23, 1911.

Tanaka, M., V. Sladek, and J. Sladek, Regularization techniques applied to boundary element methods, *Appl. Mech. Rev.*, *47*, 457–499, 1994.

Thomas, A. L., and D. D. Pollard, The geometry of echelon fractures in rock: Implications from laboratory and numerical experiments, *J. Struct. Geol.*, *15*, 323–334, 1993.

J. R. Lister, Institute of Theoretical Geophysics, Department of Applied Mathematics and Theoretical Physics, University of Cambridge, Silver Street, Cambridge CB3 9EW, UK. (lister@esc.cam.ac.uk)

C. Mériaux, Research School of Earth Sciences, Australian National University, Mills Road, Canberra, ACT 0200, Australia. (meriaux@rses.anu.edu.au)